

Search for $b \rightarrow u$ transitions in $B^- \rightarrow D^0 K^-$ and $B^- \rightarrow D^{*0} K^-$

B. Aubert, R. Barate, D. Boutigny, F. Couderc, Y. Karyotakis, J. P. Lees, V. Poireau, V. Tisserand, and A. Zghiche
Laboratoire de Physique des Particules, F-74941 Annecy-le-Vieux, France

E. Grauges
IFAE, Universitat Autònoma de Barcelona, E-08193 Bellaterra, Barcelona, Spain

A. Palano, M. Pappagallo, and A. Pompili
Università di Bari, Dipartimento di Fisica and INFN, I-70126 Bari, Italy

J. C. Chen, N. D. Qi, G. Rong, P. Wang, and Y. S. Zhu
Institute of High Energy Physics, Beijing 100039, China

G. Eigen, I. Ofte, and B. Stugu
University of Bergen, Inst. of Physics, N-5007 Bergen, Norway

G. S. Abrams, M. Battaglia, A. W. Borgland, A. B. Breon, D. N. Brown, J. Button-Shafer,
R. N. Cahn, E. Charles, C. T. Day, M. S. Gill, A. V. Gritsan, Y. Groysman, R. G. Jacobsen,
R. W. Kadel, J. Kadyk, L. T. Kerth, Yu. G. Kolomensky, G. Kukartsev, G. Lynch, L. M. Mir,
P. J. Oddone, T. J. Orimoto, M. Pripstein, N. A. Roe, M. T. Ronan, and W. A. Wenzel
Lawrence Berkeley National Laboratory and University of California, Berkeley, California 94720, USA

M. Barrett, K. E. Ford, T. J. Harrison, A. J. Hart, C. M. Hawkes, S. E. Morgan, and A. T. Watson
University of Birmingham, Birmingham, B15 2TT, United Kingdom

M. Fritsch, K. Goetzen, T. Held, H. Koch, B. Lewandowski, M. Pelizaeus, K. Peters, T. Schroeder, and M. Steinke
Ruhr Universität Bochum, Institut für Experimentalphysik 1, D-44780 Bochum, Germany

J. T. Boyd, J. P. Burke, N. Chevalier, W. N. Cottingham, and M. P. Kelly
University of Bristol, Bristol BS8 1TL, United Kingdom

T. Cuhadar-Donszelmann, C. Hearty, N. S. Knecht, T. S. Mattison, and J. A. McKenna
University of British Columbia, Vancouver, British Columbia, Canada V6T 1Z1

A. Khan, P. Kyberd, and L. Teodorescu
Brunel University, Uxbridge, Middlesex UB8 3PH, United Kingdom

A. E. Blinov, V. E. Blinov, A. D. Bukin, V. P. Druzhinin, V. B. Golubev, V. N. Ivanchenko,
E. A. Kravchenko, A. P. Onuchin, S. I. Serednyakov, Yu. I. Skovpen, E. P. Solodov, and A. N. Yushkov
Budker Institute of Nuclear Physics, Novosibirsk 630090, Russia

D. Best, M. Bondioli, M. Bruinsma, M. Chao, I. Eschrich, D. Kirkby,
A. J. Lankford, M. Mandelkern, R. K. Mommsen, W. Roethel, and D. P. Stoker
University of California at Irvine, Irvine, California 92697, USA

C. Buchanan, B. L. Hartfiel, and A. J. R. Weinstein
University of California at Los Angeles, Los Angeles, California 90024, USA

S. D. Foulkes, J. W. Gary, O. Long, B. C. Shen, K. Wang, and L. Zhang
University of California at Riverside, Riverside, California 92521, USA

D. del Re, H. K. Hadavand, E. J. Hill, D. B. MacFarlane, H. P. Paar, S. Rahatlou, and V. Sharma
University of California at San Diego, La Jolla, California 92093, USA

J. W. Berryhill, C. Campagnari, A. Cunha, B. Dahmes,
T. M. Hong, A. Lu, M. A. Mazur, J. D. Richman, and W. Verkerke
University of California at Santa Barbara, Santa Barbara, California 93106, USA

T. W. Beck, A. M. Eisner, C. J. Flacco, C. A. Heusch, J. Kroseberg, W. S. Lockman, G. Nesom,
T. Schalk, B. A. Schumm, A. Seiden, P. Spradlin, D. C. Williams, and M. G. Wilson
University of California at Santa Cruz, Institute for Particle Physics, Santa Cruz, California 95064, USA

J. Albert, E. Chen, G. P. Dubois-Felsmann, A. Dvoretzkii, D. G. Hitlin,
I. Narsky, T. Piatenko, F. C. Porter, A. Ryd, and A. Samuel
California Institute of Technology, Pasadena, California 91125, USA

R. Andreassen, S. Jayatilleke, G. Mancinelli, B. T. Meadows, and M. D. Sokoloff
University of Cincinnati, Cincinnati, Ohio 45221, USA

F. Blanc, P. Bloom, S. Chen, W. T. Ford, U. Nauenberg, A. Olivas, P. Rankin,
W. O. Ruddick, J. G. Smith, K. A. Ulmer, S. R. Wagner, and J. Zhang
University of Colorado, Boulder, Colorado 80309, USA

A. Chen, E. A. Eckhart, J. L. Harton, A. Soffer, W. H. Toki, R. J. Wilson, and Q. Zeng
Colorado State University, Fort Collins, Colorado 80523, USA

B. Spaan
Universität Dortmund, Institut für Physik, D-44221 Dortmund, Germany

D. Altenburg, T. Brandt, J. Brose, M. Dickopp, E. Feltresi, A. Hauke, V. Kloze, H. M. Lacker, E. Maly,
R. Nogowski, S. Otto, A. Petzold, G. Schott, J. Schubert, K. R. Schubert, R. Schwierz, and J. E. Sundermann
Technische Universität Dresden, Institut für Kern- und Teilchenphysik, D-01062 Dresden, Germany

D. Bernard, G. R. Bonneaud, P. Grenier, S. Schrenk, Ch. Thiebaux, G. Vasileiadis, and M. Verderi
Ecole Polytechnique, LLR, F-91128 Palaiseau, France

D. J. Bard, P. J. Clark, W. Gradl, F. Muheim, S. Playfer, and Y. Xie
University of Edinburgh, Edinburgh EH9 3JZ, United Kingdom

M. Andreotti, V. Azzolini, D. Bettoni, C. Bozzi, R. Calabrese, G. Cibinetto, E. Luppi, M. Negrini, and L. Piemontese
Università di Ferrara, Dipartimento di Fisica and INFN, I-44100 Ferrara, Italy

F. Anulli, R. Baldini-Ferrolì, A. Calcaterra, R. de Sangro,
G. Finocchiaro, P. Patteri, I. M. Peruzzi, M. Piccolo, and A. Zallo
Laboratori Nazionali di Frascati dell'INFN, I-00044 Frascati, Italy

A. Buzzo, R. Capra, R. Contri, M. Lo Vetere, M. Macri, M. R. Monge,
S. Passaggio, C. Patrignani, E. Robutti, A. Santroni, and S. Tosi
Università di Genova, Dipartimento di Fisica and INFN, I-16146 Genova, Italy

S. Bailey, G. Brandenburg, K. S. Chaisanguanthum, M. Morii, and E. Won
Harvard University, Cambridge, Massachusetts 02138, USA

R. S. Dubitzky, U. Langenegger, J. Marks, S. Schenk, and U. Uwer
Universität Heidelberg, Physikalisches Institut, Philosophenweg 12, D-69120 Heidelberg, Germany

W. Bhimji, D. A. Bowerman, P. D. Dauncey, U. Egede, R. L. Flack,
J. R. Gaillard, G. W. Morton, J. A. Nash, M. B. Nikolich, and G. P. Taylor
Imperial College London, London, SW7 2AZ, United Kingdom

M. J. Charles, G. J. Grenier, U. Mallik, and A. K. Mohapatra

University of Iowa, Iowa City, Iowa 52242, USA

J. Cochran, H. B. Crawley, V. Eyges, W. T. Meyer, S. Prell, E. I. Rosenberg, A. E. Rubin, and J. Yi
Iowa State University, Ames, Iowa 50011-3160, USA

N. Arnaud, M. Davier, X. Giroux, G. Grosdidier, A. Höcker, F. Le Diberder, V. Lepeltier, A. M. Lutz, A. Oyanguren,
T. C. Petersen, M. Pierini, S. Plaszczynski, S. Rodier, P. Roudeau, M. H. Schune, A. Stocchi, and G. Wormser
Laboratoire de l'Accélérateur Linéaire, F-91898 Orsay, France

C. H. Cheng, D. J. Lange, M. C. Simani, and D. M. Wright
Lawrence Livermore National Laboratory, Livermore, California 94550, USA

A. J. Bevan, C. A. Chavez, J. P. Coleman, I. J. Forster, J. R. Fry, E. Gabathuler,
R. Gamet, K. A. George, D. E. Hutchcroft, R. J. Parry, D. J. Payne, and C. Touramanis
University of Liverpool, Liverpool L69 72E, United Kingdom

C. M. Cormack and F. Di Lodovico
Queen Mary, University of London, E1 4NS, United Kingdom

C. L. Brown, G. Cowan, H. U. Flaecher, M. G. Green, P. S. Jackson, T. R. McMahon, S. Ricciardi, and F. Salvatore
University of London, Royal Holloway and Bedford New College, Egham, Surrey TW20 0EX, United Kingdom

D. Brown and C. L. Davis
University of Louisville, Louisville, Kentucky 40292, USA

J. Allison, N. R. Barlow, R. J. Barlow, M. C. Hodgkinson, G. D. Lafferty, M. T. Naisbit, and J. C. Williams
University of Manchester, Manchester M13 9PL, United Kingdom

C. Chen, A. Farbin, W. D. Hulsbergen, A. Jawahery, D. Kovalskyi, C. K. Lae, V. Lillard, and D. A. Roberts
University of Maryland, College Park, Maryland 20742, USA

G. Blaylock, C. Dallapiccola, S. S. Hertzbach, R. Kofler, V. B. Koptchev,
X. Li, T. B. Moore, S. Saremi, H. Staengle, and S. Willocq
University of Massachusetts, Amherst, Massachusetts 01003, USA

R. Cowan, K. Koeneke, G. Sciolla, S. J. Sekula, F. Taylor, and R. K. Yamamoto
Massachusetts Institute of Technology, Laboratory for Nuclear Science, Cambridge, Massachusetts 02139, USA

H. Kim, P. M. Patel, and S. H. Robertson
McGill University, Montréal, Quebec, Canada H3A 2T8

A. Lazzaro, V. Lombardo, and F. Palombo
Università di Milano, Dipartimento di Fisica and INFN, I-20133 Milano, Italy

J. M. Bauer, L. Cremaldi, V. Eschenburg, R. Godang, R. Kroeger,
J. Reidy, D. A. Sanders, D. J. Summers, and H. W. Zhao
University of Mississippi, University, Mississippi 38677, USA

S. Brunet, D. Côté, P. Taras, and B. Viaud
Université de Montréal, Laboratoire René J. A. Lévesque, Montréal, Quebec, Canada H3C 3J7

H. Nicholson
Mount Holyoke College, South Hadley, Massachusetts 01075, USA

N. Cavallo,* G. De Nardo, F. Fabozzi,* C. Gatto, L. Lista, D. Monorchio, P. Paolucci, D. Piccolo, and C. Sciacca
Università di Napoli Federico II, Dipartimento di Scienze Fisiche and INFN, I-80126, Napoli, Italy

M. Baak, H. Bulten, G. Raven, H. L. Snoek, and L. Wilden

NIKHEF, National Institute for Nuclear Physics and High Energy Physics, NL-1009 DB Amsterdam, The Netherlands

C. P. Jessop and J. M. LoSecco
University of Notre Dame, Notre Dame, Indiana 46556, USA

T. Allmendinger, G. Benelli, K. K. Gan, K. Honscheid, D. Hufnagel, P. D. Jackson,
H. Kagan, R. Kass, T. Pulliam, A. M. Rahimi, R. Ter-Antonyan, and Q. K. Wong
Ohio State University, Columbus, Ohio 43210, USA

J. Brau, R. Frey, O. Igonkina, M. Lu, C. T. Potter, N. B. Sinev, D. Strom, and E. Torrence
University of Oregon, Eugene, Oregon 97403, USA

F. Colechia, A. Dorigo, F. Galeazzi, M. Margoni, M. Morandin,
M. Posocco, M. Rotondo, F. Simonetto, R. Stroili, and C. Voci
Università di Padova, Dipartimento di Fisica and INFN, I-35131 Padova, Italy

M. Benayoun, H. Briand, J. Chauveau, P. David, L. Del Buono, Ch. de la Vaissière,
O. Hamon, M. J. J. John, Ph. Leruste, J. Malclès, J. Ocariz, L. Roos, and G. Therin
Universités Paris VI et VII, Laboratoire de Physique Nucléaire et de Hautes Energies, F-75252 Paris, France

P. K. Behera, L. Gladney, Q. H. Guo, and J. Panetta
University of Pennsylvania, Philadelphia, Pennsylvania 19104, USA

M. Biasini, R. Covarelli, S. Pacetti, and M. Pioppi
Università di Perugia, Dipartimento di Fisica and INFN, I-06100 Perugia, Italy

C. Angelini, G. Batignani, S. Bettarini, F. Bucci, G. Calderini, M. Carpinelli, F. Forti, M. A. Giorgi,
A. Lusiani, G. Marchiori, M. Morganti, N. Neri, E. Paoloni, M. Rama, G. Rizzo, G. Simi, and J. Walsh
Università di Pisa, Dipartimento di Fisica, Scuola Normale Superiore and INFN, I-56127 Pisa, Italy

M. Haire, D. Judd, K. Paick, and D. E. Wagoner
Prairie View A&M University, Prairie View, Texas 77446, USA

J. Biesiada, N. Danielson, P. Elmer, Y. P. Lau, C. Lu, J. Olsen, A. J. S. Smith, and A. V. Telnov
Princeton University, Princeton, New Jersey 08544, USA

F. Bellini, G. Cavoto, A. D’Orazio, E. Di Marco, R. Faccini, F. Ferrarotto, F. Ferroni, M. Gaspero,
L. Li Gioi, M. A. Mazzoni, S. Morganti, G. Piredda, F. Polci, F. Safai Tehrani, and C. Voena
Università di Roma La Sapienza, Dipartimento di Fisica and INFN, I-00185 Roma, Italy

S. Christ, H. Schröder, G. Wagner, and R. Waldi
Universität Rostock, D-18051 Rostock, Germany

T. Adye, N. De Groot, B. Franek, G. P. Gopal, E. O. Olaiya, and F. F. Wilson
Rutherford Appleton Laboratory, Chilton, Didcot, Oxon, OX11 0QX, United Kingdom

R. Aleksan, S. Emery, A. Gaidot, S. F. Ganzhur, P.-F. Giraud, G. Graziani, G. Hamel de Monchenault,
W. Kozanecki, M. Legendre, G. W. London, B. Mayer, G. Vasseur, Ch. Yèche, and M. Zito
DSM/Dapnia, CEA/Saclay, F-91191 Gif-sur-Yvette, France

M. V. Purohit, A. W. Weidemann, J. R. Wilson, and F. X. Yumiceva
University of South Carolina, Columbia, South Carolina 29208, USA

T. Abe, M. T. Allen, D. Aston, R. Bartoldus, N. Berger, A. M. Boyarski, O. L. Buchmueller, R. Claus,
M. R. Convery, M. Cristinziani, J. C. Dingfelder, D. Dong, J. Dorfan, D. Dujmic, W. Dunwoodie, S. Fan,
R. C. Field, T. Glanzman, S. J. Gowdy, T. Hadig, V. Halyo, C. Hast, T. Hryn’ova, W. R. Innes, M. H. Kelsey,
P. Kim, M. L. Kocian, D. W. G. S. Leith, J. Libby, S. Luitz, V. Luth, H. L. Lynch, H. Marsiske, R. Messner,

D. R. Muller, C. P. O'Grady, V. E. Ozcan, A. Perazzo, M. Perl, B. N. Ratcliff, A. Roodman, A. A. Salnikov, R. H. Schindler, J. Schwiening, A. Snyder, J. Stelzer, D. Su, M. K. Sullivan, K. Suzuki, J. M. Thompson, J. Va'vra, M. Weaver, W. J. Wisniewski, M. Wittgen, D. H. Wright, A. K. Yarritu, K. Yi, and C. C. Young
Stanford Linear Accelerator Center, Stanford, California 94309, USA

J. Strube
*University of Oregon, Eugene, Oregon 97403, USA and
Stanford Linear Accelerator Center, Stanford, California 94309, USA*

P. R. Burchat, A. J. Edwards, S. A. Majewski, B. A. Petersen, and C. Roat
Stanford University, Stanford, California 94305-4060, USA

M. Ahmed, S. Ahmed, M. S. Alam, J. A. Ernst, M. A. Saeed, M. Saleem, F. R. Wappler, and S. B. Zain
State University of New York, Albany, New York 12222, USA

W. Bugg, M. Krishnamurthy, and S. M. Spanier
University of Tennessee, Knoxville, Tennessee 37996, USA

R. Eckmann, J. L. Ritchie, A. Satpathy, and R. F. Schwitters
University of Texas at Austin, Austin, Texas 78712, USA

J. M. Izen, I. Kitayama, X. C. Lou, and S. Ye
University of Texas at Dallas, Richardson, Texas 75083, USA

F. Bianchi, M. Bona, F. Gallo, and D. Gamba
Università di Torino, Dipartimento di Fisica Sperimentale and INFN, I-10125 Torino, Italy

M. Bomben, L. Bosisio, C. Cartaro, F. Cossutti, G. Della Ricca, S. Dittongo,
S. Grancagnolo, L. Lanceri, P. Poropat,[†] L. Vitale, and G. Vuagnin
Università di Trieste, Dipartimento di Fisica and INFN, I-34127 Trieste, Italy

F. Martinez-Vidal
IFIC, Universitat de Valencia-CSIC, E-46071 Valencia, Spain

R. S. Panvini[†]
Vanderbilt University, Nashville, Tennessee 37235, USA

Sw. Banerjee, B. Bhuyan, C. M. Brown, D. Fortin, K. Hamano, R. Kowalewski, J. M. Roney, and R. J. Sobie
University of Victoria, Victoria, British Columbia, Canada V8W 3P6

J. J. Back, P. F. Harrison, T. E. Latham, and G. B. Mohanty
Department of Physics, University of Warwick, Coventry CV4 7AL, United Kingdom

H. R. Band, X. Chen, B. Cheng, S. Dasu, M. Datta, A. M. Eichenbaum, K. T. Flood,
M. Graham, J. J. Hollar, J. R. Johnson, P. E. Kutter, H. Li, R. Liu, B. Mellado, A. Mihalyi,
Y. Pan, R. Prepost, P. Tan, J. H. von Wimmersperg-Toeller, J. Wu, S. L. Wu, and Z. Yu
University of Wisconsin, Madison, Wisconsin 53706, USA

M. G. Greene and H. Neal
Yale University, New Haven, Connecticut 06511, USA

We search for $B^- \rightarrow \tilde{D}^0 K^-$ and $B^- \rightarrow \tilde{D}^{*0} K^-$ and charge conjugates. Here the symbol \tilde{D}^0 indicates decay of a D^0 or \bar{D}^0 into $K^+ \pi^-$, while the symbol \tilde{D}^{*0} indicates decay of a D^{*0} or \bar{D}^{*0} to $\tilde{D}^0 \pi^0$ or $\tilde{D}^0 \gamma$. These final states can be reached through the $b \rightarrow c$ transition $B^- \rightarrow D^{(*)0} K^-$ followed by the doubly Cabibbo-Kobayashi-Maskawa (CKM)-suppressed $D^0 \rightarrow K^+ \pi^-$, or the $b \rightarrow u$ transition $B^- \rightarrow \bar{D}^{(*)0} K^-$ followed by the CKM-favored $\bar{D}^0 \rightarrow K^+ \pi^-$. The interference of these two amplitudes is sensitive to the angle γ of the unitarity triangle. Our results are based on 232 million $\Upsilon(4S) \rightarrow B\bar{B}$ decays collected with the BABAR detector at SLAC. We find no significant evidence for these decays. We set a limit $r_B \equiv |A(B^- \rightarrow \bar{D}^0 K^-)/A(B^- \rightarrow D^0 K^-)| < 0.23$ at

90% C.L. using the most conservative assumptions on the values of the CKM angle γ and the strong phases in the B and D decay amplitudes. In the case of the D^* we set a 90% C.L. limit $r_B^{*2} \equiv |A(B^- \rightarrow \bar{D}^{*0} K^-)/A(B^- \rightarrow D^{*0} K^-)|^2 < (0.16)^2$ which is independent of assumptions on γ and strong phases.

PACS numbers: 13.25.Hw, 14.40.Nd

I. INTRODUCTION

Following the discovery of CP violation in B -meson decays and the measurement of the angle β of the unitarity triangle [1] associated with the Cabibbo-Kobayashi-Maskawa (CKM) quark mixing matrix, focus has turned towards the measurements of the other angles α and γ . The angle γ is $\arg(-V_{ub}^* V_{ud}/V_{cb}^* V_{cd})$, where V_{ij} are CKM matrix elements. In the Wolfenstein convention [2], $\gamma = \arg(V_{ub}^*)$.

Several proposed methods for measuring γ exploit the interference between $B^- \rightarrow D^{(*)0} K^{(*)-}$ and $B^- \rightarrow \bar{D}^{(*)0} K^{(*)-}$ (Fig. 1) that occurs when the $D^{(*)0}$ and the $\bar{D}^{(*)0}$ decay to common final states, as first suggested in Ref. [3].

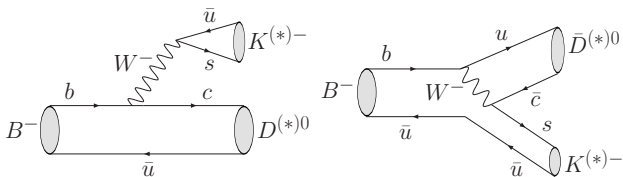


FIG. 1: Feynman diagrams for $B^- \rightarrow D^{(*)0} K^{(*)-}$ and $B^- \rightarrow \bar{D}^{(*)0} K^{(*)-}$. The latter is CKM and color suppressed with respect to the former. The CKM-suppression factor is $|V_{ub} V_{cs}^*/V_{cb} V_{us}^*| \approx 0.4$. The naive color-suppression factor is $\frac{1}{3}$.

As proposed in Ref. [4], we search for $B^- \rightarrow \tilde{D}^0 K^-$ and $B^- \rightarrow \tilde{D}^{*0} K^-$, $\tilde{D}^{*0} \rightarrow \tilde{D}^0 \pi^0$ or $\tilde{D}^{*0} \rightarrow \tilde{D}^0 \gamma$, followed by $\tilde{D}^0 \rightarrow K^+ \pi^-$, as well as the charge conjugate (c.c.) sequences. Here the symbol \tilde{D}^0 indicates the decay of a D^0 or \bar{D}^0 into $K^+ \pi^-$. In these processes, the favored B decay ($B^- \rightarrow D^{(*)0} K^-$) followed by the doubly CKM-suppressed D decay ($D^0 \rightarrow K^+ \pi^-$) interferes with the suppressed B decay ($B^- \rightarrow \bar{D}^{(*)0} K^-$) followed by the CKM-favored D decay ($\bar{D}^0 \rightarrow K^+ \pi^-$). The interference of the $b \rightarrow c$ ($B^- \rightarrow D^{(*)0} K^-$) and $b \rightarrow u$ ($B^- \rightarrow \bar{D}^{(*)0} K^-$) amplitudes is sensitive to the relative weak phase γ .

We use the notation $B^- \rightarrow [h_1^+ h_2^-]_D h_3^-$ (with each $h_i = \pi$ or K) for the decay chain $B^- \rightarrow \tilde{D}^0 h_3^-$, $\tilde{D}^0 \rightarrow h_1^+ h_2^-$. For the closely related modes with a \tilde{D}^{*0} , we use the same notation with the subscript D replaced by $D\pi^0$

or $D\gamma$, depending on whether the \tilde{D}^{*0} decays to $\tilde{D}^0 \pi^0$ or $\tilde{D}^0 \gamma$. We also refer to h_3 as the bachelor π or K .

In the decays of interest, the sign of the bachelor kaon is opposite to that of the kaon from \tilde{D}^0 decay. It is convenient to define ratios of rates between these decays and the similar decays where the two kaons have the same sign. The decays with same-sign kaons have much higher rate and proceed almost exclusively through the CKM-favored and color-favored B transition, followed by the CKM-favored D -decay, e.g., $B^- \rightarrow D^0 K^-$, $D^0 \rightarrow K^- \pi^+$. The advantage of taking ratios is that most theoretical and experimental uncertainties cancel. Thus, ignoring possible small effects due to D mixing and taking into account the effective phase difference of π between the D^* decays in $D\gamma$ and $D\pi^0$ [5], we define the charge-specific ratios for D and D^* as:

$$\mathcal{R}_{K\pi}^\pm \equiv \frac{\Gamma([K^\mp \pi^\pm]_{D\pi^0} K^\pm)}{\Gamma([K^\pm \pi^\mp]_{D\pi^0} K^\pm)} = r_B^2 + r_D^2 + 2r_B r_D \cos(\pm\gamma + \delta), \quad (1)$$

$$\begin{aligned} \mathcal{R}_{K\pi, D\pi^0}^{*\pm} &\equiv \frac{\Gamma([K^\mp \pi^\pm]_{D\pi^0} K^\pm)}{\Gamma([K^\pm \pi^\mp]_{D\pi^0} K^\pm)} \\ &= r_B^{*2} + r_D^2 + 2r_B^* r_D \cos(\pm\gamma + \delta^*), \end{aligned} \quad (2)$$

and

$$\begin{aligned} \mathcal{R}_{K\pi, D\gamma}^{*\pm} &\equiv \frac{\Gamma([K^\mp \pi^\pm]_{D\gamma} K^\pm)}{\Gamma([K^\pm \pi^\mp]_{D\gamma} K^\pm)} \\ &= r_B^{*2} + r_D^2 - 2r_B^* r_D \cos(\pm\gamma + \delta^*), \end{aligned} \quad (3)$$

where

$$r_B \equiv \left| \frac{A(B^- \rightarrow \bar{D}^0 K^-)}{A(B^- \rightarrow D^0 K^-)} \right|, \quad (4)$$

$$r_B^* \equiv \left| \frac{A(B^- \rightarrow \bar{D}^{*0} K^-)}{A(B^- \rightarrow D^{*0} K^-)} \right|, \quad (5)$$

$$r_D \equiv \left| \frac{A(D^0 \rightarrow K^+ \pi^-)}{A(D^0 \rightarrow K^- \pi^+)} \right|, \quad (6)$$

$$\delta^{(*)} \equiv \delta_B^{(*)} + \delta_D, \quad (7)$$

and $\delta_B^{(*)}$ and δ_D are strong phase differences between the two B and D decay amplitudes, respectively. The value of r_D has been measured to be $r_D = 0.060 \pm 0.002$ [6].

*Also with Università della Basilicata, Potenza, Italy

†Deceased

We also define the charge-independent ratio

$$\mathcal{R}_{K\pi} \equiv \frac{\Gamma([K^+\pi^-]_D K^-) + \Gamma([K^-\pi^+]_D K^+)}{\Gamma([K^-\pi^+]_D K^-) + \Gamma([K^+\pi^-]_D K^+)} \quad (8)$$

and the equivalent ratios for the D^* modes,

$$\mathcal{R}_{K\pi, D\pi^0} \equiv \frac{\Gamma([K^+\pi^-]_{D\pi^0} K^-) + \Gamma([K^-\pi^+]_{D\pi^0} K^+)}{\Gamma([K^-\pi^+]_{D\pi^0} K^-) + \Gamma([K^+\pi^-]_{D\pi^0} K^+)}, \quad (9)$$

and

$$\mathcal{R}_{K\pi, D\gamma} \equiv \frac{\Gamma([K^+\pi^-]_{D\gamma} K^-) + \Gamma([K^-\pi^+]_{D\gamma} K^+)}{\Gamma([K^-\pi^+]_{D\gamma} K^-) + \Gamma([K^+\pi^-]_{D\gamma} K^+)}. \quad (10)$$

Then,

$$\mathcal{R}_{K\pi} = \frac{\mathcal{R}_{K\pi}^+ + \mathcal{R}_{K\pi}^-}{2} = r_B^2 + r_D^2 + 2r_B r_D \cos \gamma \cos \delta \quad (11)$$

and, similarly for the D^* modes,

$$\mathcal{R}_{K\pi, D\pi^0}^* = r_B^{*2} + r_D^2 + 2r_B^* r_D \cos \gamma \cos \delta^*, \quad (12)$$

$$\mathcal{R}_{K\pi, D\gamma}^* = r_B^{*2} + r_D^2 - 2r_B^* r_D \cos \gamma \cos \delta^*. \quad (13)$$

Equations 11, 12, and 13 assume no CP violation in the normalization modes $[K^\mp \pi^\pm]_D K^\mp$, $[K^\mp \pi^\pm]_{D\pi^0} K^\mp$, and $[K^\mp \pi^\pm]_{D\gamma} K^\mp$. In the following we use the notation $\mathcal{R}_{K\pi}^*$ when there is no need to refer specifically to $\mathcal{R}_{K\pi, D\pi^0}^*$ or $\mathcal{R}_{K\pi, D\gamma}^*$.

As discussed below, the parameter $r_B^{(*)}$ is expected to be of the same order as r_D . Thus, CP violation could manifest itself as a large difference between the charge-specific ratios $\mathcal{R}_{K\pi}^{(*)+}$ and $\mathcal{R}_{K\pi}^{(*)-}$. Measurements of these six ratios can be used to constrain γ .

The value of $r_B^{(*)}$ determines, in part, the level of interference between the diagrams of Fig. 1. In most techniques for measuring γ , high values of $r_B^{(*)}$ lead to larger interference and better sensitivity to γ . Thus, r_B and r_B^* are key quantities whose values have a significant impact on the ability to measure the CKM angle γ at the B -factories and beyond.

In the standard model, $r_B^{(*)} = |V_{ub} V_{cs}^* / V_{cb} V_{us}^*| F_{cs} \approx 0.4 F_{cs}$. The color-suppression factor $F_{cs} < 1$ accounts for the additional suppression, beyond that due to CKM factors, of $B^- \rightarrow \bar{D}^{(*)0} K^-$ relative to $B^- \rightarrow D^{(*)0} K^-$. Naively, $F_{cs} = \frac{1}{3}$, which is the probability for the color of the quarks from the virtual W in $B^- \rightarrow \bar{D}^{(*)0} K^-$ to match that of the other two quarks; see Fig. 1. Early estimates [7] of F_{cs} were based on factorization and the experimental information on a number of $b \rightarrow c$ transitions available at the time. These estimates gave $F_{cs} \approx 0.22$, leading to $r_B^{(*)} \approx 0.09$. However, the recent observations and measurements [8] of color-suppressed $b \rightarrow c$ decays ($B \rightarrow D^{(*)} h^0$; $h^0 = \pi^0, \rho^0, \omega, \eta, \eta'$) suggest that color suppression is not as effective as anticipated, and therefore the value of $r_B^{(*)}$ could be of order 0.2 [9].

As we will describe below, the measured $\mathcal{R}_{K\pi}^{(*)}$ are consistent with zero in the current analysis. Since $\mathcal{R}_{K\pi}^{(*)}$ depend quadratically on $r_B^{(*)}$, we will use our measurements to set restrictive upper limits on $r_B^{(*)}$.

It is important to note the different signs of the third terms in the expressions for $\mathcal{R}_{K\pi, D\pi^0}^*$ and $\mathcal{R}_{K\pi, D\gamma}^*$ in Equations 12 and 13. This relative minus sign is due to the phase of π between the two D^* decay modes [5]. It allows for a measurement of r_B^* with no additional inputs since $r_B^{*2} = \frac{1}{2}(\mathcal{R}_{D\pi^0}^* + \mathcal{R}_{D\gamma}^*) - r_D^2$, and r_D is known quite precisely ($r_D = 0.060 \pm 0.002$). We will use this equation for r_B^* and our results for $\mathcal{R}_{D\pi^0}^*$ and $\mathcal{R}_{D\gamma}^*$ to set an upper limit on r_B^* with no assumptions.

On the other hand, $\mathcal{R}_{K\pi}$ depends on the three unknowns r_B , γ , and δ , see Equation 11; thus, in order to extract a limit on r_B from the experimental limit on $\mathcal{R}_{K\pi}$ we must make assumptions about γ and δ . As we will discuss in Section IV, we have chosen to quote an upper limit on r_B based on the most conservative assumptions on γ and δ .

In this paper we report on an update of our previous search for $B^- \rightarrow \bar{D}^0 K^-$ [10], and the first attempt to study $B^- \rightarrow \bar{D}^{*0} K^-$. The previous analysis was based on a sample of B -meson decays a factor of 1.9 smaller than used here, and resulted in an upper limit $\mathcal{R}_{K\pi} < 0.026$ at the 90% C.L. This in turn was translated into a limit $r_B < 0.22$, also at the 90% confidence level. A similar analysis by the Belle Collaboration [11] gives limits $\mathcal{R}_{K\pi} < 0.044$ and $r_B < 0.27$ (90% C.L.).

Information on r_B , r_B^* , and γ can also be obtained from studies of $B^\pm \rightarrow \bar{D}^0 K^\pm$ and $B^\pm \rightarrow \bar{D}^{*0} K^\pm$, $\bar{D}^0 \rightarrow K_S \pi^+ \pi^-$. An analysis by the Belle collaboration [12] finds quite large values $r_B = 0.31 \pm 0.11$ and $r_B^* = 0.34 \pm 0.14$, although the uncertainties are large enough that these results are not inconsistent with the limits listed above. On the other hand, a similar analysis by the BABAR Collaboration [13] favors smaller values for these amplitude ratios: $r_B = 0.12 \pm 0.09$ at 90% C.L. and $r_B^* = 0.17 \pm 0.10$.

II. THE BABAR DATASET

The results presented in this paper are based on $232 \times 10^6 \Upsilon(4S) \rightarrow B\bar{B}$ decays, corresponding to an integrated luminosity of 211 fb^{-1} . The data were collected between 1999 and 2004 with the BABAR detector [14] at the PEP-II B Factory at SLAC [15]. In addition, a 16 fb^{-1} off-resonance data sample, with center-of-mass (CM) energy 40 MeV below the $\Upsilon(4S)$ resonance, is used to study backgrounds from continuum events, $e^+e^- \rightarrow q\bar{q}$ ($q = u, d, s$, or c).

TABLE I: Notation used in the text for the decay modes that define the data samples used in the analysis.

Abbreviation	Mode	Comments
DK	$B^- \rightarrow D^0 K^-, D^0 \rightarrow K^- \pi^+$ and c.c.	normalization
$D\pi$	$B^- \rightarrow D^0 \pi^-, D^0 \rightarrow K^- \pi^+$ and c.c.	control
$\bar{D}K$	$B^- \rightarrow \bar{D}^0 K^-, \bar{D}^0 \rightarrow K^+ \pi^-$ and c.c.	signal
D^*K	$B^- \rightarrow D^{*0} K^-, D^{*0} \rightarrow D^0 \pi^0/\gamma, D^0 \rightarrow K^- \pi^+$ and c.c.	normalization
$D^*\pi$	$B^- \rightarrow D^{*0} \pi^-, D^{*0} \rightarrow D^0 \pi^0/\gamma, D^0 \rightarrow K^- \pi^+$ and c.c.	control
\bar{D}^*K	$B^- \rightarrow \bar{D}^{*0} K^-, \bar{D}^{*0} \rightarrow \bar{D}^0 \pi^0/\gamma, \bar{D}^0 \rightarrow K^+ \pi^-$ and c.c.	signal

III. ANALYSIS METHOD

This work is an extension of our analysis from Ref. [10], which resulted in 90% C.L. limits on $\mathcal{R}_{K\pi} < 0.026$ and $r_B < 0.22$, as mentioned in Section I. The main changes in the analysis are the following:

- The size of the dataset is increased from 120 to 232×10^6 $\Upsilon(4S) \rightarrow B\bar{B}$ decays.
- This analysis also includes the $B^\pm \rightarrow \tilde{D}^{*0} K^\pm$ mode.
- The event selection criteria have been made more stringent in order to reduce backgrounds further.
- A few of the selection criteria in the previous analysis resulted in small differences in the efficiencies of the signal mode $B^\pm \rightarrow [K^\mp \pi^\pm]_D K^\pm$ and the normalization mode $B^\pm \rightarrow [K^\pm \pi^\mp]_D K^\pm$. These selection criteria have now been removed.

The analysis makes use of several samples from different decay modes. Throughout the following discussion we will refer to these modes using abbreviations that are summarized in Table I.

The event selection is developed from studies of simulated $B\bar{B}$ and continuum events, and off-resonance data. A large on-resonance control sample of $D\pi$ and $D^*\pi$ events is used to validate several aspects of the simulation and analysis procedure.

The analysis strategy is the following:

1. The goal is to measure or set limits on the charge-independent ratios $\mathcal{R}_{K\pi}$ and $\mathcal{R}_{K^*\pi}$.
2. The first step consists of the application of a set of basic selection criteria to select possible candidate events, see Section III A.
3. After the basic selection criteria, the backgrounds are dominantly from continuum. These are significantly reduced with a neural network designed to distinguish between $B\bar{B}$ and continuum events, see Section III B.
4. After the neural network requirement, events are characterized by two kinematical variables that are customarily used when reconstructing B -meson decays at the $\Upsilon(4S)$. These variables are the energy-substituted mass, $m_{\text{ES}} \equiv$

$\sqrt{(\frac{s}{2} + \vec{p}_0 \cdot \vec{p}_B)^2 / E_0^2 - p_B^2}$ and energy difference $\Delta E \equiv E_B^* - \frac{1}{2}\sqrt{s}$, where E and p are energy and momentum, the asterisk denotes the CM frame, the subscripts 0 and B refer to the $\Upsilon(4S)$ and B candidate, respectively, and s is the square of the CM energy. For signal events $m_{\text{ES}} = m_B$ and $\Delta E = 0$ within the resolution of about 2.5 and 20 MeV, respectively (here m_B is the known B mass [6]).

5. We then perform simultaneous unbinned maximum likelihood fits to the final signal samples ($\bar{D}K$ and \bar{D}^*K), the normalization samples (DK and D^*K), and the control samples ($D\pi$ and $D^*\pi$) to extract $\mathcal{R}_{K\pi}$ and $\mathcal{R}_{K^*\pi}$, see Section III C. The fits are based on the reconstructed values of m_{ES} and ΔE in the various event samples.
6. Throughout the whole analysis chain, care is taken to treat the signal, normalization, and control samples in a consistent manner.

A. Basic Selection Criteria

Charged kaon and pion candidates in the decay modes of interest must satisfy K or π identification criteria [16] that are typically 85% efficient, depending on momentum and polar angle. The misidentification rates are at the few percent level.

The invariant mass of the $K\pi$ pair must be within 18.8 MeV (2.5σ) of the mean reconstructed D^0 mass (1863.3 MeV). For modes with $\tilde{D}^{*0} \rightarrow \tilde{D}^0 \pi^0$ and $\tilde{D}^{*0} \rightarrow \tilde{D}^0 \gamma$ the mass difference ΔM between the \tilde{D}^{*0} and the \tilde{D}^0 must be within 3.5 MeV (3.5σ) and 13 MeV (2σ), respectively, of the expectation for \tilde{D}^{*0} decays (142.2 MeV).

A major background arises from DK and D^*K decays in which the K and π in the D decay are misidentified as π and K , respectively. When this happens, the decay could be reconstructed as a $\bar{D}K$ or \bar{D}^*K signal event. To eliminate this background, we recompute the invariant mass (M_{switch}) of the $h^+ h^-$ pair in $\tilde{D}^0 \rightarrow h^+ h^-$ switching the particle identification assumptions (π vs. K) on the h^+ and the h^- . We veto any candidates with M_{switch} within 18 MeV of the known D mass [6]; this requirement is 90% efficient on signal decays. In the case of $\tilde{D}^0 K$, we also veto any candidate for which the \tilde{D}^0 is consistent with $D^{*+} \rightarrow D^0 \pi^+$ or $D^{*0} \rightarrow D^0 \pi^0$ decay.

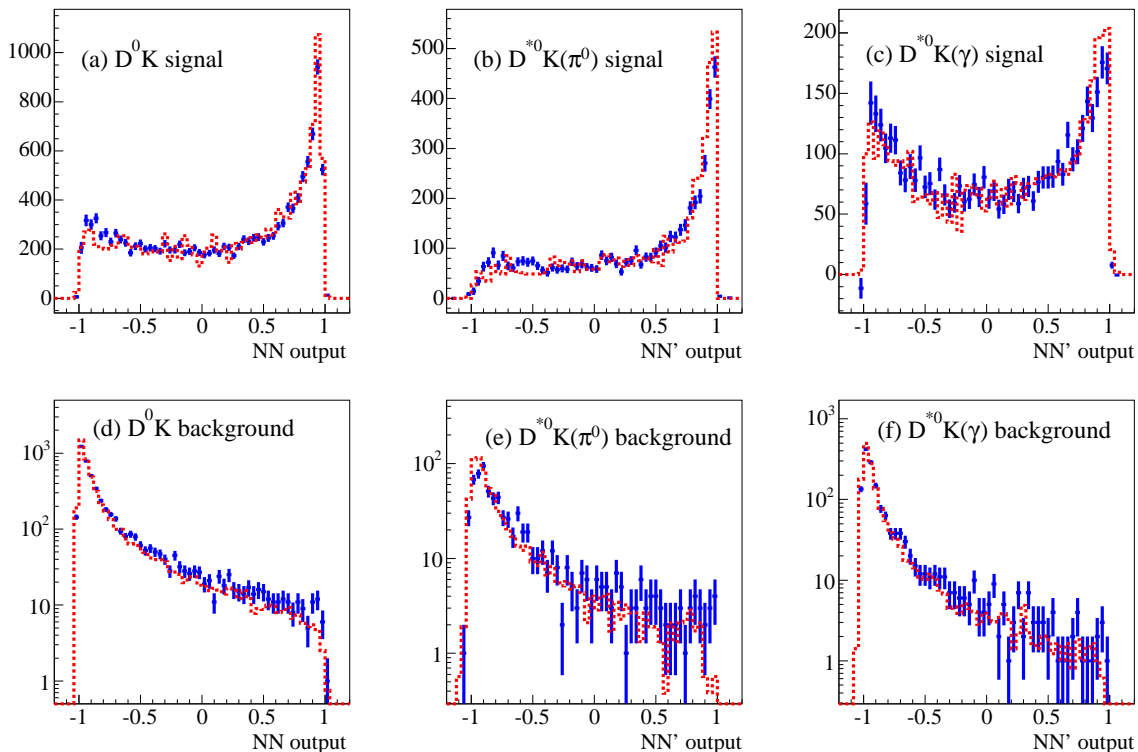


FIG. 2: Distributions of the continuum suppression neural network (NN and NN') outputs for the three modes. Figs. (a-c) show the expected distribution from signal events. The dashed line histogram shows the distribution of simulated signal events and the histogram with error bars shows the distribution of $D^{(*)0}\pi$ control sample events with background subtracted using the m_{ES} sideband ($5.20 \text{ GeV} < m_{ES} < 5.27 \text{ GeV}$). Figs. (d-f) show the expected distribution for continuum background events. The dashed line histogram shows the distribution of simulated continuum events and the histogram with errors shows the distribution of off-resonance events. The m_{ES} and ΔE requirements on the off-resonance and continuum Monte Carlo events have been kept loose to increase the statistics. Each Monte Carlo histogram is normalized to the area of the corresponding data histogram.

B. Neural Network

After these initial selection criteria, backgrounds are overwhelmingly from continuum events, especially $e^+e^- \rightarrow c\bar{c}$, with $\bar{c} \rightarrow \bar{D}^0 X$, $\bar{D}^0 \rightarrow K^+\pi^-$ and $c \rightarrow DX$, $D \rightarrow K^-Y$.

The continuum background is reduced using a neural network technique. The neural network algorithms used for the modes with and without a D^* are slightly different. First, for all modes we use a common neural network (NN) based on nine quantities, listed below, that distinguish between continuum and $B\bar{B}$ events. Then, for the modes with a D^* we also take advantage of the fact that the signal is distributed as $\cos^2\theta_{D^*}$ for $D^* \rightarrow D\pi$ or $\sin^2\theta_{D^*}$ for $D^* \rightarrow D\gamma$, while the background is roughly independent of $\cos\theta_{D^*}$. Here θ_{D^*} is the decay angle of the D^* , *i.e.*, the angle between the direction of the D and the line of flight of the D^* relative to the parent B , evaluated in the D^* rest frame. Thus, we construct a second neural network, NN' , which takes as inputs the output of NN and the value of $\cos\theta_{D^*}$. We then use as

a selection requirement the output of NN in the $\tilde{D}^0 K$ analysis and the output of NN' in the $\tilde{D}^{*0} K$ analysis.

The nine variables used in defining NN are the following:

1. A Fisher discriminant [17] constructed from the quantities $L_0 = \sum_i p_i$ and $L_2 = \sum_i p_i \cos^2\theta_i$ calculated in the CM frame. Here, p_i is the momentum and θ_i the angle with respect to the thrust axis of the B candidate of tracks and clusters not used to reconstruct the B meson.
2. $|\cos\theta_T|$, where θ_T is the angle in the CM frame between the thrust axes of the B candidate and the detected remainder of the event. The distribution of $|\cos\theta_T|$ is approximately flat for signal and strongly peaked at one for continuum background.
3. $\cos\theta_B^*$, where θ_B^* is the polar angle of the B candidate in the CM frame. In this variable, the signal follows a $\sin^2\theta_B^*$ distribution, while the background is approximately uniform.

4. $\cos\theta_D^K$ where θ_D^K is the decay angle in $\tilde{D}^0 \rightarrow K\pi$.
5. $\cos\theta_B^{D^{(*)}}$, where $\theta_B^{D^{(*)}}$ is the decay angle in $B \rightarrow \tilde{D}^0 K$ or $B \rightarrow \tilde{D}^{*0} K$. In signal events the distributions of $\cos\theta_D^K$ and $\cos\theta_B^{D^{(*)}}$ are uniform. On the other hand, the corresponding distributions in combinatorial background events tend to show accumulations of events near the extreme values.
6. The charge difference ΔQ between the sum of the charges of tracks in the \tilde{D}^0 or \tilde{D}^{*0} hemisphere and the sum of the charges of the tracks in the opposite hemisphere excluding those tracks used in the reconstructed B . The partitioning of the event in the two hemispheres is done in the CM frame. For signal, $\langle\Delta Q\rangle = 0$, whereas for the $c\bar{c}$ background $\langle\Delta Q\rangle \approx \frac{7}{3} \times Q_B$, where Q_B is the charge of the B candidate. The value of $\langle\Delta Q\rangle$ in $c\bar{c}$ events is a consequence of the correlation between the charge of the c (or \bar{c}) in a given hemisphere and the sum of the charges of all particles in that hemisphere. Since the ΔQ RMS is 2.4, this variable provides approximately a 1σ separation between signal and $c\bar{c}$ background.
7. $Q_B \cdot Q_K$, where Q_K is the sum of the charges of all kaons not in the reconstructed B , and Q_B , as defined above, is the charge of the reconstructed B candidate. In many signal events, there is a charged kaon among the decay products of the other B in the event. The charge of this kaon tends to be highly correlated with the charge of the B . Thus, signal events tend to have $Q_B \cdot Q_K \leq -1$. On the other hand, most continuum events have no kaons outside of the reconstructed B , and therefore $Q_K = 0$.
8. The distance of closest approach between the bachelor track and the trajectory of the \tilde{D}^0 . This is consistent with zero for signal events, but can be larger in $c\bar{c}$ events.
9. A quantity $\mathcal{M}_{K\ell}$ defined to be zero if there are no leptons (e or μ) in the event, one if there is a lepton in the event and the invariant mass ($m_{K\ell}$) of this lepton and the bachelor kaon is less than the mass of the D -meson (m_D), and two if $m_{K\ell} > m_D$. This quantity differentiates between continuum and signal events because the probability of finding a lepton in a continuum event is smaller than in a $B\bar{B}$ event. Furthermore, a large fraction of leptons in $c\bar{c}$ events are from $D \rightarrow K\ell\nu$, where K is reconstructed as the bachelor kaon. For these events $m_{K\ell} < m_D$, while in signal events the expected distribution of $m_{K\ell}$ extends to larger values.

The neural networks (NN and NN') are trained with simulated continuum and signal events. The distributions of the NN and NN' outputs for the control samples ($D\pi$, $D^*\pi$, and off resonance data) are compared

with expectations from the Monte Carlo simulation in Fig. 2. The agreement is satisfactory. We have also examined the distributions of all variables used in NN and NN' , and found good agreement between the simulation and the data control samples.

Our final event selection requirement is $NN > 0.5$ for $\bar{D}K$ and $NN' > 0.5$ for \bar{D}^*K . In addition, to reduce the remaining $B\bar{B}$ backgrounds, we also require $\cos\theta_D^K > -0.75$. These final requirements are about 40% efficient on simulated signal events, and reject 98.5% of the continuum background.

The overall reconstruction efficiencies, estimated from Monte Carlo simulation, are about 14% for $\bar{D}K$, 8% for \bar{D}^*K with $\bar{D}^* \rightarrow \bar{D}\pi^0$ and 7% for \bar{D}^*K with $\bar{D}^* \rightarrow \bar{D}\gamma$. Note that a precise knowledge of the efficiencies is not needed in the analysis. We apply the identical requirements to the normalization modes DK and D^*K . Then, in the extraction of $\mathcal{R}_{K\pi}$ and $\mathcal{R}_{K\pi}^*$, the efficiencies of the overall selection cancel in the ratio.

C. Fitting for event yields and $\mathcal{R}_{K\pi}^{(*)}$

The ratios $\mathcal{R}_{K\pi}$ and $\mathcal{R}_{K\pi}^*$ are extracted from the ratios of the event yields in the m_{ES} distribution for the signal modes ($\bar{D}K$ and \bar{D}^*K) and the normalization modes (DK and D^*K), taking into account potential differences in efficiencies and backgrounds. All events must satisfy the requirements discussed above and have a ΔE value consistent with zero within the resolution ($-52 \text{ MeV} < \Delta E < 44 \text{ MeV}$). Here we discuss the procedure to extract $\mathcal{R}_{K\pi}$; the values of $\mathcal{R}_{K\pi, D\pi^0}^*$ and $\mathcal{R}_{K\pi, D\gamma}^*$ are obtained in the same way.

The m_{ES} distributions for $\bar{D}K$ (signal mode) and DK (normalization mode) are fitted simultaneously. The fit parameter $\mathcal{R}_{K\pi}$ is given by $\mathcal{R}_{K\pi} \equiv c \cdot N_{\bar{D}K} / N_{DK}$, where $N_{\bar{D}K}$ and N_{DK} are the fitted yields of $\bar{D}K$ and DK events, and c is a correction factor, determined from Monte Carlo, for the ratio of efficiencies between the two modes. We find that this factor c is consistent with unity within the statistical accuracy of the simulation, $c = 0.98 \pm 0.04$ (these correction factors are $c = 0.97 \pm 0.05$ and $c = 0.99 \pm 0.05$ for $D^* \rightarrow D\pi^0$ and $D^* \rightarrow D\gamma$, respectively).

The m_{ES} distributions are modeled as the sum of a threshold combinatorial background function [18] and a Gaussian lineshape centered at m_B . The parameters of the background function for the signal mode are constrained by a simultaneous fit of the m_{ES} distribution for events in the sideband of ΔE ($-120 \text{ MeV} < \Delta E < 200 \text{ MeV}$, excluding the ΔE signal region defined above). The parameters of the Gaussian for the signal and normalization modes are taken to be identical. The number of events in the Gaussian is $N_{sig} + N_{peak}$, where $N_{sig} = N_{DK}$ or $N_{\bar{D}K}$ and N_{peak} is the number of background events expected to be distributed in the same way as DK or $\bar{D}K$ in m_{ES} (“peaking backgrounds”).

There are two classes of peaking background events:

TABLE II: Summary of fit results.

Mode	$\bar{D}K$	$\bar{D}^*K, \bar{D}^* \rightarrow \bar{D}\pi^0$	$\bar{D}^*K, \bar{D}^* \rightarrow \bar{D}\gamma$
Ratio of rates, $\mathcal{R}_{K\pi}$ or $\mathcal{R}_{K^*\pi}^*$, $\times 10^{-3}$	$\mathcal{R}_{K\pi} = 13_{-9}^{+11}$	$\mathcal{R}_{K\pi}^* = -2_{-6}^{+10}$	$\mathcal{R}_{K\pi}^* = 11_{-13}^{+18}$
Number of signal events	5_{-3}^{+4}	$-0.2_{-0.7}^{+1.3}$	$1.2_{-1.4}^{+2.1}$
Number of normalization events	368 ± 26	150 ± 17	108 ± 14
Number of peaking charmless events	$0.7_{-0.7}^{+1.4}$	$0.0_{-0.0}^{+0.3}$	$0.1_{-0.1}^{+0.8}$
Number of peaking $D^{(*)}\pi$ events in signal sample	0.48 ± 0.05	0.18 ± 0.03	0.01 ± 0.02

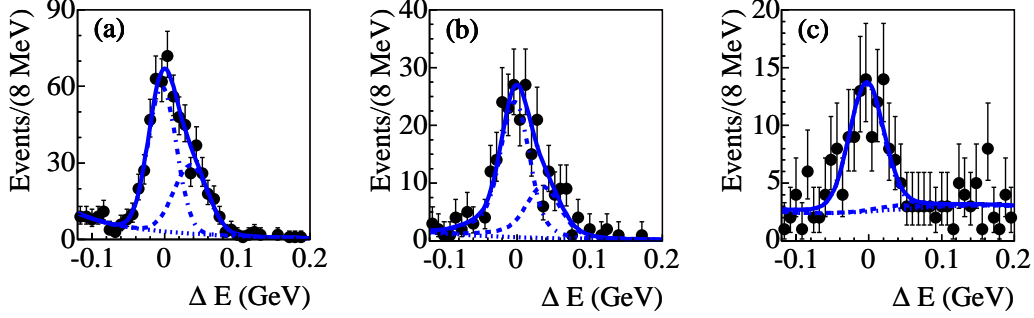


FIG. 3: ΔE distributions for normalization events (DK and D^*K) with m_{ES} within 3σ of m_B with the fit model overlaid. (a) DK events. (b) D^*K events with $D^* \rightarrow D\pi^0$. (c) D^*K events with $D^* \rightarrow D\gamma$. The dashed (dot-dashed) lines are the contributions from $D\pi$ or $D^*\pi$ (DK or D^*K) events. The dotted lines are the contributions from other backgrounds, and the solid line is the total.

1. Charmless B decays, *e.g.*, $B^- \rightarrow K^+K^-\pi^+$. These are indistinguishable from the $\bar{D}K$ signal if the $K^-\pi^+$ pair happens to be consistent with the D mass.
2. Events of the type $B^- \rightarrow D^0\pi^-$, where the bachelor π^- is misidentified as a K^- . When the D^0 decays into $K^-\pi^+$ ($K^+\pi^-$), these events are indistinguishable in m_{ES} from DK ($\bar{D}K$), since m_{ES} is independent of particle identification assumptions.

The amount of peaking charmless B background (1) is estimated directly from the data by performing a simultaneous fit to events in the sideband of the reconstructed D mass. In this fit the number of charmless background events is constrained to be ≥ 0 .

The ΔE distribution of the $D\pi$ background (2) is shifted by about +50 MeV due to the misidentification of the bachelor π as a K . Since the ΔE resolution is of order 20 MeV, the ΔE requirement does not eliminate this background completely. The remaining $D\pi$ background after the ΔE requirement is estimated relaxing the ΔE requirement and performing a fit to the ΔE distribution of the DK candidate sample, as described below.

We fit the ΔE distribution of DK candidates, with m_{ES} within 3σ of m_B , to the sum of a DK component, a $D\pi$ background component, and a combinatorial background component, see Fig. 3. From this fit we can estimate the number of $D\pi$ background events after the ΔE requirement, which we denote as N_{DK}^π . In this fit,

the ΔE shapes of the DK and $D\pi$ components are constrained from the data as follows:

- The large $D\pi$ sample, with the bachelor track identified as a pion, is used to constrain the shape of the DK component in the sample of DK candidates.
- The same sample of $D\pi$ events, but reconstructed as DK events, is used to constrain the shape of the $D\pi$ background in the DK sample.

The $D\pi$ peaking background is much more important in the DK (normalization) channel than in the $\bar{D}K$ (signal) channel. This is because in order to contribute to the signal channel, the D^0 has to decay into $K^+\pi^-$, and this mode is doubly CKM suppressed. For the $\bar{D}K$ (signal) sample, the contribution from the residual $D\pi$ peaking background in the m_{ES} fit is estimated as $N_{\bar{D}K}^\pi = r_D^2 N_{DK}^\pi$, where $r_D = 0.060 \pm 0.002$ is the ratio of the doubly CKM-suppressed to the CKM-favored $D \rightarrow K\pi$ amplitudes and N_{DK}^π was defined above.

The complete procedure simultaneously fits seven distributions: the m_{ES} distributions of DK and $\bar{D}K$, the $\bar{D}K$ distributions in sidebands of ΔE and $m(D^0)$, the ΔE distribution of DK , and the ΔE distributions of $D\pi$ reconstructed as $D\pi$ and as DK . All fits are unbinned extended maximum likelihood fits. They are configured in such a way that $\mathcal{R}_{K\pi}$ and $\mathcal{R}_{K^*\pi}^*$ are explicit fit parameters. The advantage of this approach is that all uncertainties, including the uncertainties in the PDFs and

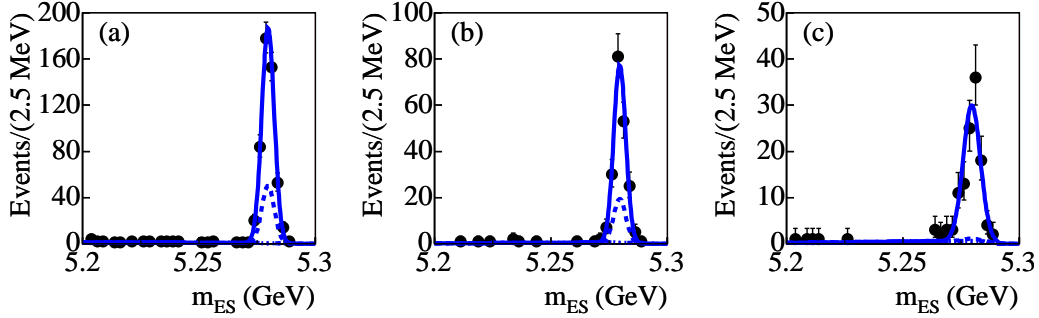


FIG. 4: m_{ES} distributions for normalization events (DK and D^*K) with ΔE in the signal region with the fit model overlaid. (a) DK events. (b) D^*K events with $D^* \rightarrow D\pi^0$. (c) D^*K events with $D^* \rightarrow D\gamma$. The dashed lines represent the backgrounds; these are mostly from $D\pi$ or $D^*\pi$, and also peak at the B -mass. As explained in the text, the size of the $D\pi$ and $D^*\pi$ backgrounds is constrained by the simultaneous fits to the distributions of Fig. 3.

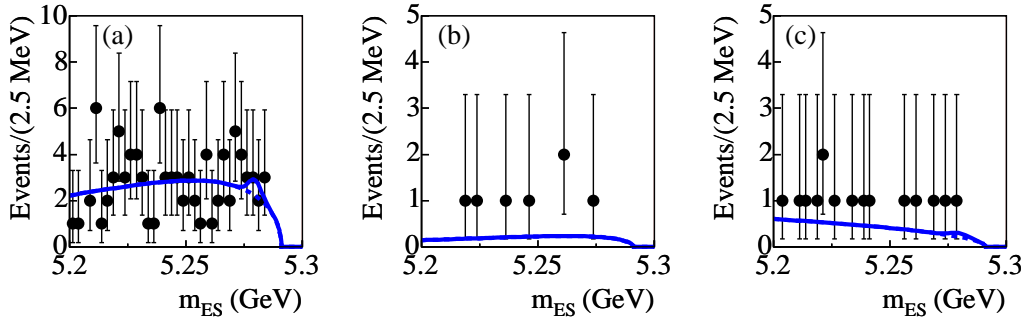


FIG. 5: m_{ES} distributions for $\bar{D}K$ and \bar{D}^*K events with $K\pi$ mass in a sideband of the reconstructed D mass and with ΔE in the signal region. These events are used to constrain the size of possible peaking backgrounds from charmless B -meson decays, *i.e.*, decays without a D in the final state. The fit model is overlaid. (a) $\bar{D}K$ events. (b) \bar{D}^*K events with $D^* \rightarrow D\pi^0$. (c) \bar{D}^*K events with $D^* \rightarrow D\gamma$. Note that the $K\pi$ mass range in the sideband selection is a factor of 2.7 larger than in the signal selection.

the uncertainties in the background subtractions, are correctly propagated in the statistical uncertainty reported by the fit.

The fit is performed separately for $\bar{D}K$, \bar{D}^*K , $\bar{D}^* \rightarrow \bar{D}\pi^0$, and \bar{D}^*K , $\bar{D}^* \rightarrow \bar{D}\gamma$ and is identical for all three modes, except in the choice of parameterization for some signal and background components in the ΔE fits.

Systematic uncertainties in the detector efficiency cancel in the ratio. This cancellation has been verified by studies of simulated events, with a statistical precision of a few percent. The likelihood includes a Gaussian uncertainty term for this cancellation which is set by the statistical accuracy of the simulation. Other systematic uncertainties, *e.g.*, the uncertainty in the parameter r_D used to estimate the amount of peaking backgrounds from $D^{(*)}\pi$, are also included in the formulation of the likelihood.

The fit procedure has been extensively tested on sets of simulated events. It was found to provide an unbiased estimation of the parameters $\mathcal{R}_{K\pi}$ and $\mathcal{R}_{K^*\pi}$.

IV. RESULTS

The results of the fits are displayed in Table II and Figs. 3, 4, 5, and 6. As is apparent from Fig. 6, we see no evidence for the \bar{D}^*K and $\bar{D}K$ modes.

For the $\bar{D}K$ mode we find $\mathcal{R}_{K\pi} = (13_{-9}^{+11}) \times 10^{-3}$; for the \bar{D}^*K mode we find $\mathcal{R}_{K\pi, D\pi^0}^* = (-2_{-6}^{+10}) \times 10^{-3}$ (for $D^* \rightarrow D\pi^0$) and $\mathcal{R}_{K\pi, D\gamma}^* = (11_{-13}^{+18}) \times 10^{-3}$ (for $D^* \rightarrow D\gamma$).

Next, we use our measurements to extract information on r_B and r_B^* . In the case of decays into \bar{D}^{*0} we start from equations 12 and 13 to derive

$$r_B^{*2} = \frac{\mathcal{R}_{K\pi, D\pi^0}^* + \mathcal{R}_{K\pi, D\gamma}^*}{2} - r_D^2. \quad (14)$$

We use the relationship given by equation 14 in conjunction with $r_D = 0.060 \pm 0.002$ and our results for $\mathcal{R}_{K\pi, D\pi^0}^*$ and $\mathcal{R}_{K\pi, D\gamma}^*$ to extract information on r_B^{*2} with no assumptions on the values of γ and strong phases.

Since the uncertainties in $\mathcal{R}_{K\pi, D\pi^0}^*$ and $\mathcal{R}_{K\pi, D\gamma}^*$ are non-Gaussian, care must be taken in propagating them

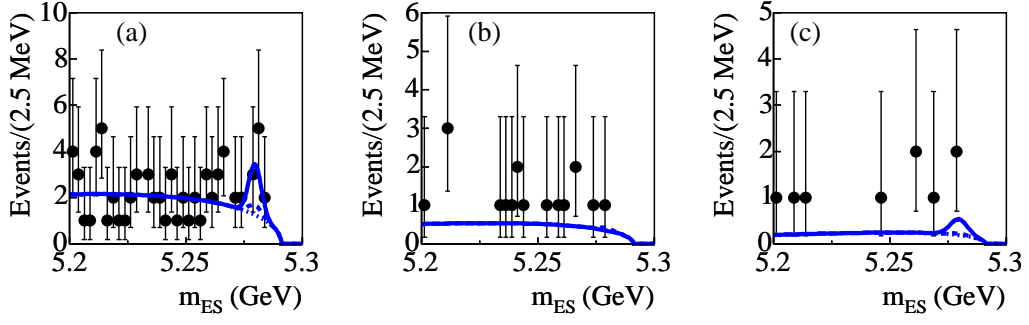


FIG. 6: m_{ES} distributions for candidate signal events with the fit model overlaid. (a) $\bar{D}K$ events. (b) \bar{D}^*K events with $D^* \rightarrow D\pi^0$. (c) \bar{D}^*K events with $D^* \rightarrow D\gamma$.

into an uncertainty in r_B^{*2} . We interpret the fit likelihoods for $\mathcal{R}_{K\pi, D\pi^0}^*$ and $\mathcal{R}_{K\pi, D\gamma}^*$ (see Figure 7) as posterior PDFs assuming constant priors. We assume a Gaussian PDF for r_D . We then convolve numerically the three PDFs for $\mathcal{R}_{K\pi, D\pi^0}^*$, $\mathcal{R}_{K\pi, D\gamma}^*$, and r_D according to equation 14 to obtain a PDF for r_B^{*2} which is shown in Figure 8. The convolution relies on the fact that the measurements of $\mathcal{R}_{K\pi, D\pi^0}^*$ and $\mathcal{R}_{K\pi, D\gamma}^*$ are uncorrelated (the correlation due to the uncertainty in r_D , which was used to extract the $D\pi$ peaking backgrounds in the two modes, is negligible).

Our result is $r_B^{*2} = (4_{-8}^{+14}) \times 10^{-3}$. Based on the PDF for r_B^{*2} shown in Figure 8 we set an upper limit $r_B^{*2} < (0.16)^2$ at the 90% C.L. using a Bayesian method with a uniform prior for $r_B^{*2} > 0$.

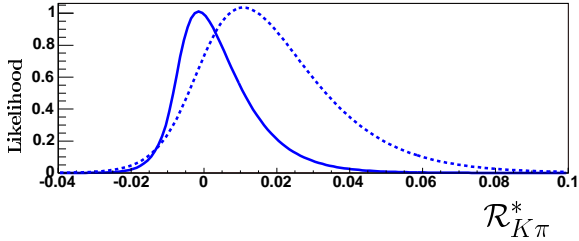


FIG. 7: Likelihood functions as obtained from the fit described in the text for $\mathcal{R}_{K\pi, D\pi^0}^*$ (solid line) and $\mathcal{R}_{K\pi, D\gamma}^*$ (dashed line).

In the case of decays into a D/\bar{D} , there is not enough information to extract the ratio r_B without additional assumptions. Thus, we first extract an upper limit on the experimentally measured quantity $\mathcal{R}_{K\pi}$. This is done starting from the likelihood as a function of $\mathcal{R}_{K\pi}$ (see Fig. 9) using a Bayesian method with a uniform prior for $\mathcal{R}_{K\pi} > 0$. The limit is $\mathcal{R}_{K\pi} < 0.029$ at 90% C.L. Next, in Fig. 10 we show the dependence of $\mathcal{R}_{K\pi}$ on r_B , together with our limit on $\mathcal{R}_{K\pi}$. This dependence is shown allowing a $\pm 1\sigma$ variation on r_D , for the full range $0^\circ - 180^\circ$ for γ and δ , as well as with the restriction

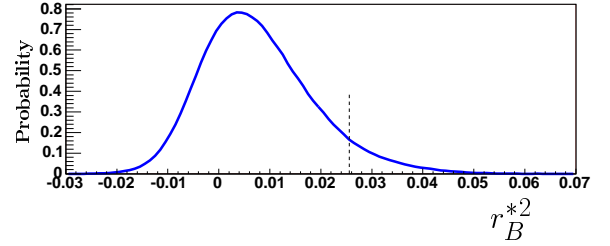


FIG. 8: Probability distribution function (arbitrary units) for r_B^{*2} obtained as described in the text. The integral of the function for $0 < r_B^{*2} < (0.16)^2$ is nine-tenths of the integral for $r_B^{*2} > 0$. The vertical dashed line is drawn at $r_B^{*2} = (0.16)^2$.

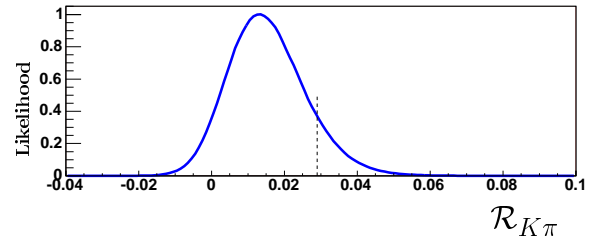


FIG. 9: Likelihood function (arbitrary units) for $\mathcal{R}_{K\pi}$ as extracted from the fit described in the text. The integral of the likelihood function for $0 < \mathcal{R}_{K\pi} < 0.029$ is nine-tenths of the integral for $\mathcal{R}_{K\pi} > 0$. The vertical dashed line is drawn at $\mathcal{R}_{K\pi} = 0.029$.

$51^\circ < \gamma < 66^\circ$ suggested by global CKM fits [19]. We use the information displayed in this Figure to set an upper limit on r_B . The least restrictive limit on r_B is computed assuming maximal destructive interference between the $b \rightarrow c$ and $b \rightarrow u$ amplitudes: $\gamma = 0^\circ, \delta = 180^\circ$ or $\gamma = 180^\circ, \delta = 0^\circ$. The limit is $r_B < 0.23$ at 90% C.L.

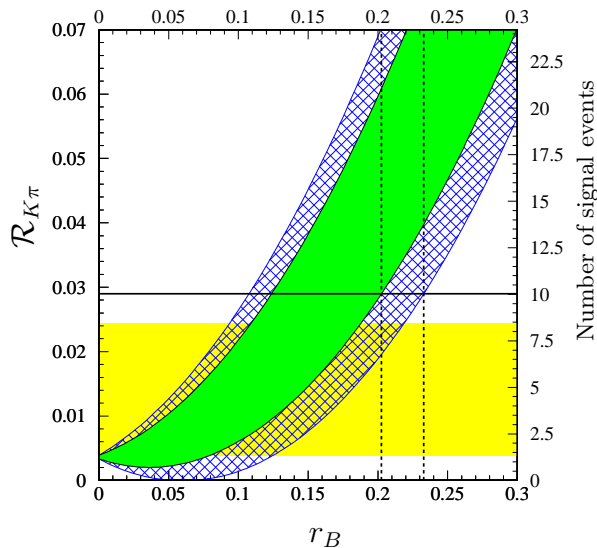


FIG. 10: Expectations for $\mathcal{R}_{K\pi}$ and the number of signal events *vs.* r_B . Dark filled-in area: allowed region for any value of δ , with a $\pm 1\sigma$ variation on r_D , and $51^\circ < \gamma < 66^\circ$. Hatched area: additional allowed region with no constraint on γ . Note that the uncertainty on r_D has a very small effect on the size of the allowed regions. The horizontal line represents the 90% C.L. limit $\mathcal{R}_{K\pi} < 0.029$. The vertical dashed lines are drawn at $r_B = 0.203$ and $r_B = 0.233$. They represent the 90% C.L. upper limits on r_B with and without the constraint on γ . The light filled-in area represents the 68% C.L. region corresponding to $\mathcal{R}_{K\pi} = 0.013 \pm_{0.009}^{0.011}$.

TABLE III: Summary of the results of this analysis.

	Measured Value	90% C.L. limit
$\mathcal{R}_{K\pi}$	$0.013 \pm_{0.009}^{0.011}$	< 0.029
$\mathcal{R}_{K\pi, D\pi^0}^*$	$-0.002 \pm_{0.006}^{0.010}$	< 0.023
$\mathcal{R}_{K\pi, D\gamma}^*$	$0.011 \pm_{0.013}^{0.018}$	< 0.045
r_B	...	< 0.23
r_B^{*2}	$0.004 \pm_{0.008}^{0.014}$	$< (0.16)^2$

V. SUMMARY

In summary, we find no significant evidence for the decays $B^\pm \rightarrow [K^\mp \pi^\pm]_D K^\pm$ and $B^\pm \rightarrow [K^\mp \pi^\pm]_{D^*} K^\pm$.

We set upper limits on the ratios $\mathcal{R}_{K\pi}^{(*)}$ of the rates for these modes and the favored modes $B^\pm \rightarrow [K^\pm \pi^\mp]_D K^\pm$ and $B^\pm \rightarrow [K^\pm \pi^\mp]_{D^*} K^\pm$. We also use our data to set upper limits on the ratios of $b \rightarrow u$ and $b \rightarrow c$ amplitudes r_B and r_B^* . All of our results are summarized in Table III.

Our results favor values of r_B and r_B^* somewhat smaller than the value of 0.2 which can be estimated from the measurements of color-suppressed $b \rightarrow c$ transitions [9]. If r_B and r_B^* are small, the suppression of the $b \rightarrow u$ amplitude will make the determination of γ using methods based on the interference of the diagrams in Fig. 1 difficult.

VI. ACKNOWLEDGMENTS

We are grateful for the extraordinary contributions of our PEP-II colleagues in achieving the excellent luminosity and machine conditions that have made this work possible. The success of this project also relies critically on the expertise and dedication of the computing organizations that support *BABAR*. The collaborating institutions wish to thank SLAC for its support and the kind hospitality extended to them. This work is supported by the US Department of Energy and National Science Foundation, the Natural Sciences and Engineering Research Council (Canada), Institute of High Energy Physics (China), the Commissariat à l'Énergie Atomique and Institut National de Physique Nucléaire et de Physique des Particules (France), the Bundesministerium für Bildung und Forschung and Deutsche Forschungsgemeinschaft (Germany), the Istituto Nazionale di Fisica Nucleare (Italy), the Foundation for Fundamental Research on Matter (The Netherlands), the Research Council of Norway, the Ministry of Science and Technology of the Russian Federation, and the Particle Physics and Astronomy Research Council (United Kingdom). Individuals have received support from CONACyT (Mexico), the A. P. Sloan Foundation, the Research Corporation, and the Alexander von Humboldt Foundation.

-
- [1] *BABAR* Collaboration, B. Aubert *et al.*, Phys. Rev. Lett. **89**, 201802 (2002); Belle Collaboration, K. Abe *et al.*, Phys. Rev. **D66**, 071102 (2002).
[2] L. Wolfenstein, Phys. Rev. Lett. **51**, 1945 (1983).
[3] M. Gronau and D. Wyler, Phys. Lett. **B265**, 172 (1991); M. Gronau and D. London, Phys. Lett. **B253**, 483 (1991).
[4] D. Atwood, I. Dunietz, and A. Soni, Phys. Rev. Lett. **78**,

- 3257 (1997); Phys. Rev. **D63**, 036005 (2001).
[5] A. Bondar and T. Gershon, Phys. Rev. **D70**, 091503 (2004).
[6] Particle Data Group, S. Eidelman *et al.*, Phys. Lett. **B592**, 1 (2004).
[7] See, for example, M. Neubert and B. Stech, in *Heavy Flavours*, edited by A.J. Buras and M. Lindner, World Scientific, Singapore, 1997, 2nd ed..

- [8] CLEO Collaboration, T.E. Coan *et al.*, Phys. Rev. Lett. **88**, 062001 (2002). Belle Collaboration, K. Abe *et al.*, Phys. Rev. Lett. **88**, 052002 (2002); A. Satpathy *et al.*, Phys. Lett. **B553**, 159 (2003). BABAR Collaboration, B. Aubert *et al.*, Phys. Rev. **D69**, 032004 (2004).
- [9] M. Gronau, Phys. Lett. **B557**, 198 (2003).
- [10] BABAR Collaboration, B. Aubert *et al.*, Phys. Rev. Lett. **93**, 131804 (2004).
- [11] Belle Collaboration, M. Saigo *et al.*, Phys. Rev. Lett. **94**, 091601 (2005).
- [12] Belle Collaboration, A. Poluetkov *et al.*, Phys. Rev **D70**, 072003 (2004).
- [13] BABAR Collaboration, B. Aubert *et al.*, `hep-ex/0504039`, submitted to Phys. Rev. Lett.
- [14] BABAR Collaboration, B. Aubert *et al.*, Nucl. Instr. and Methods Phys. Res., Sect. **A479**, 1 (2002).
- [15] PEP-II Conceptual Design Report, SLAC-0418 (1993).
- [16] BABAR Collaboration, B. Aubert *et al.*, Phys. Rev. **D66**, 032003 (2002).
- [17] R. A. Fisher, Ann. of Eugenics **7**, 179 (1936).
- [18] The function is $f(m_{ES}) \propto m_{ES} \sqrt{1-x^2} \exp[-\zeta(1-x^2)]$, where $x = 2m_{ES}/\sqrt{s}$ and ζ is a fit parameter; ARGUS Collaboration, H. Albrecht *et al.*, Z. Phys. **C48**, 543 (1990).
- [19] J. Charles *et al.*, Eur. Phys. J **C41**, 1 (2005); updated results can be found at <http://ckmfitter.in2p3.fr>.